


C. R. Bocking · M. G. Blyth 

# Oxygen uptake and denitrification in soil aggregates

This paper is dedicated to the memory of Franz Ziegler

Received: 16 February 2017 / Revised: 7 July 2017 / Published online: 15 November 2017  
© The Author(s) 2017. This article is an open access publication

**Abstract** A mathematical model of oxygen uptake by bacteria in agricultural soils is presented with the goal of predicting anaerobic regions in which denitrification occurs. In an environment with a plentiful supply of oxygen, micro-organisms consume oxygen through normal respiration. When the local oxygen concentration falls below a threshold level, denitrification may take place leading to the release of nitrous oxide, a potent agent for global warming. A two-dimensional model is presented in which one or more circular soil aggregates are located at a distance below the ground level at which the prevailing oxygen concentration is prescribed. The level of denitrification is estimated by computing the area of any anaerobic cores, which may develop in the interior of the aggregates. The oxygen distribution throughout the model soil is calculated first for an aggregated soil for which the ratio of the oxygen diffusivities between an aggregate and its surround is small via an asymptotic analysis. Second, the case of a non-aggregated soil featuring one or more microbial hotspots, for which the diffusion ratio is arbitrary, is examined numerically using the boundary-element method. Calculations with multiple aggregates demonstrate a sheltering effect whereby some aggregates receive less oxygen than their neighbours. In the case of an infinite regular triangular network representing an aggregated soil, it is shown that there is an optimal inter-aggregate spacing which minimises the total anaerobic core area.

## 1 Introduction

In a soil environment where the rate of uptake of oxygen through normal respiration is greater than the rate at which it is replaced from the atmosphere through diffusion, micro-organisms can instead generate energy from nitrate,  $\text{NO}_3^-$ . This process is known as anaerobic denitrification (for a review, see Knowles [19]). As a result of denitrification, nitrate is converted to nitrogen gas,  $\text{N}_2$ , via the sequence of steps (e.g. Smith et al. [30]):



Nitrous oxide ( $\text{N}_2\text{O}$ ) is created at the penultimate step and may be released in that form without being further converted into nitrogen gas. Nitrous oxide produced in this way may escape up through the ground surface and into the atmosphere, where it has a deleterious effect on stratospheric ozone and moreover poses a serious threat as a potent agent for global warming. The use of arable soils with a high nitrogen content, and the widespread use of fertilisers, has exacerbated the problem. While the levels of nitrous oxide released from soils are much smaller than the wider levels of release of carbon dioxide into the atmosphere, and while the latter is undoubtedly the most dangerous greenhouse gas, the warming potential of nitrous oxide is around 300 times greater (Houghton et al. [16]). Smith [29] notes that approximately 65% of the emissions of nitrous oxide originate from soils (for a review of the processes governing the exchange of these and other gases between

the soil and the atmosphere, see Smith et al. [30]). The notorious difficulty in measuring denitrification in the field (e.g. Groffman et al. [14]) serves to underline the need for predictive theoretical models.

Simple one-dimensional models have been proposed to quantify oxygen uptake in soils and hence act as a predictor for levels of denitrification (see, for example, Kanwar [17], Leffelaar [21], Papendick and Runkles [24] and Radford and Greenwood [27]). Typically such models assume a constant surface-level oxygen concentration at one end of the domain and include a no-flux boundary condition at the other end to represent an impermeable layer of rock at either finite or infinite depth. Greenwood [12] constructed a more sophisticated model in which an individual soil particle, hereinafter termed an aggregate, is exposed to a known uniform oxygen concentration at its surface. The aggregate is assumed to be spherical and the oxygen profile inside to be spherically symmetric. Denitrification occurs at points in the interior where the oxygen concentration falls below a threshold level, which Greenwood took to be zero. This was assumed to occur within a spherical-shaped region concentric with the aggregate boundary. Such a region is usually referred to as an anaerobic core. (We note in passing that very similar mathematical models have been constructed to study solid tumours—see, for example, Britton [4]). Greenwood and Berry [13] reported an error in Greenwood [12]’s work and extended the formulation to non-spherical aggregates. In reality, soil structure is highly complex (e.g. [9, 15]), and while models have tended to assume some symmetry for mathematical simplicity, more complex models based on fractal geometry have attempted to capture the clustering, fragmentation and stability of real soils (e.g. [25]). Models that cater for a cluster of aggregates, assuming a log-normal distribution of aggregate size and a spherically symmetric profile within each aggregate, have been proposed by Smith [28] and Arah and Smith [2].

In the present work, we present a two-dimensional model of denitrification in soils, which determines the oxygen profile in a model soil comprising multiple aggregates by solving the diffusion and uptake problems inside the aggregates and in the surround. The surface distribution of oxygen on each aggregate boundary is not known in advance and depends on the location of the aggregate beneath the ground surface and its proximity to other aggregates. We consider solitary aggregates, multiple aggregates, as well as extended networks containing a formally infinite number of individual aggregates. Oxygen is assumed to be consumed within each aggregate at a constant rate as a result of microbial action. Where the oxygen concentration falls below a prescribed level, an anaerobic core develops. The assumption of a constant uptake rate has also been adopted by a number of previous workers on the grounds of mathematical simplicity (e.g. [7, 12, 24]). Kanwar [17] notes that the take-up rate is likely to vary both with time and with depth. Radford and Greenwood [27] formulated their one-dimensional oxygen distribution problem with the uptake rate a function of the local oxygen concentration, although they assumed a constant rate in their calculations. Bocking [3] demonstrated that in the context of the two-dimensional problem to be studied in the present work, the latter assumption has little qualitative effect on the results and only a marginal quantitative effect. (A slightly larger anaerobic core is predicted in a single aggregate for constant rate of uptake.) In keeping with previous models, and with established wisdom (e.g. Currie [7]), we assume that diffusion is the dominant mechanism controlling oxygen transport within the soil and is in itself sufficient to explain the necessary gas interchange between the soil and the atmosphere (Keen [18]). By adopting a two-dimensional model, we aim to make some progress towards quantifying the effect of soil structure, namely the distribution of aggregates within the soil, on anaerobic core volume without importing the additional mathematical and computational complexity required by a fully three-dimensional approach.

Our study embraces two different viewpoints. In the first, we consider a so-called aggregated soil, which is viewed as a network of individual soil aggregates surrounded by air, or in the case of a saturated soil, water. In the alternative viewpoint, the ground is filled with soil particles (so that there are no air or water pockets), but in some parts the take-up of oxygen is effectively negligible and elsewhere there are hot spots of microbial activity causing substantial oxygen depletion (e.g. Kuzyakov and Blagodatskaya [20]). This is referred to as a non-aggregated soil (e.g. Montzka et al. [23]).

The layout of the paper is as follows: In the next section, we present our model problem for a single aggregate. In Sect. 3, we present an asymptotic analysis for an aggregated soil on the assumption the diffusion ratio between the aggregate interior and the surround is small. In Sect. 4, the case of a non-aggregated soil is examined numerically using the boundary-element method. Finally, in Sect. 5 we summarise our findings.

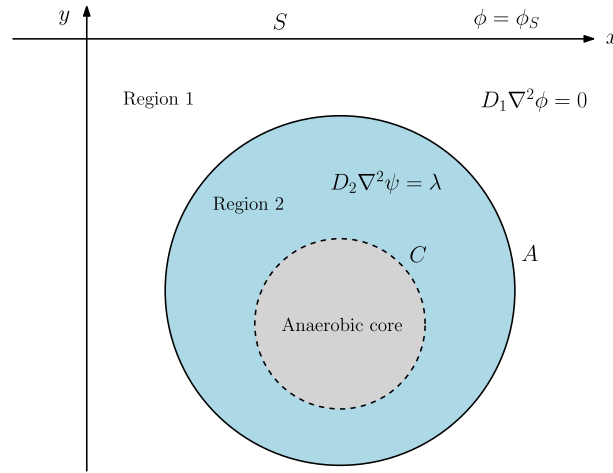


**Fig. 1** A single soil aggregate, or microbial patch, with boundary  $A$  located beneath the ground level  $S$  and containing an anaerobic core with boundary  $C$ . Oxygen diffuses throughout region 1 and diffuses and is consumed throughout region 2

**2 Statement of the model**

We consider the diffusion and consumption of oxygen within a two-dimensional soil aggregate located at a distance below ground level, as depicted in Fig. 1. We initially discuss the case of a single aggregate with a circular boundary  $A$  of radius  $a$ . The case of two or more aggregates will be considered in a later section. Referring to the set of Cartesian coordinates shown in Fig. 1, the surface of the soil (i.e. ground level), which is designated boundary  $S$ , is located at  $y = 0$ , and the centre of the aggregate is located on the vertical axis at  $y = -h$ .

An anaerobic core develops inside the aggregate when the local oxygen concentration drops below a threshold level. The boundary of this anaerobic core is labelled  $C$ . The shape and location of the free boundary  $C$  are unknown in advance and must be found as part of the solution to the problem. Although the shape of  $C$  will be determined in the ensuing analysis, it is likely to be of secondary interest in practice; our principal concern is to provide a framework for computing the anaerobic area enclosed by  $C$  to serve as a guide to the overall level of denitrification.

Outside of the soil aggregate and below ground level, which we will henceforth refer to as region 1, we assume that oxygen diffuses freely with diffusivity  $D_1$  so that the local concentration,  $\phi$ , satisfies Laplace’s equation,  $D_1 \nabla^2 \phi = 0$ . The oxygen concentration at ground level is prescribed so that  $\phi = \phi_S$ , a constant, at  $y = 0$ . Far below the aggregate we impose the condition  $\phi_y \rightarrow 0$  as  $y \rightarrow -\infty$ , so that the oxygen cannot escape downwards. Physically, we envisage a layer of rock lying some way beneath the soil through which oxygen cannot permeate. Inside the soil aggregate and outside the anaerobic core, which we will henceforth refer to as region 2, oxygen is assumed to diffuse while being consumed by bacteria at a constant rate. Accordingly the local concentration,  $\psi$ , satisfies the Poisson equation  $D_2 \nabla^2 \psi = \lambda$ , where  $\lambda$  is the rate of consumption and is subject to conditions of continuity of oxygen flux and oxygen concentration at the aggregate boundary  $A$ . The consumption rate  $\lambda$  is assumed to be constant and independent of the local oxygen concentration. At the anaerobic core boundary  $C$ , we impose a condition of zero oxygen flux together with the requirement that  $\psi = T$ , where  $T$  is the threshold value below which normal respiration ceases and denitrification occurs instead.

It is convenient to non-dimensionalise the problem using the aggregate radius  $a$  as the reference length and the ground oxygen level  $\phi_S$  as the reference concentration level. Accordingly, we obtain the dimensionless problem in region 1,

$$\nabla^2 \phi = 0, \tag{2}$$

with  $\phi = 1$  on  $S$ , and the continuity conditions on  $A$ ,

$$\phi = \psi, \quad \mathbf{n} \cdot \nabla \phi = \delta \mathbf{n} \cdot \nabla \psi, \tag{3}$$

where  $\mathbf{n}$  is the unit normal to  $A$  pointing out of the aggregate, and also the condition that  $\phi_y \rightarrow 0$  as  $y \rightarrow -\infty$ . In region 2, we have the dimensionless problem

$$\nabla^2 \psi = \alpha, \tag{4}$$

with

$$\psi = \tau, \quad \mathbf{n} \cdot \nabla \psi = 0 \tag{5}$$

on  $C$ , where  $\mathbf{n}$  is the unit normal to  $C$  pointing outwards. The pertinent dimensionless parameters are

$$\alpha = \frac{a^2 \lambda}{\phi_S D_2}, \quad \delta = \frac{D_2}{D_1}, \quad \tau = \frac{T}{\phi_S}, \quad H = \frac{h}{a}, \tag{6}$$

where the last parameter provides a measure of how far the aggregate is beneath ground level.

In general, the oxygen distribution around the boundary  $A$  will be non-uniform, the exact variation depending on the location of the aggregate relative to the ground-level surface and to any other aggregates. Fixing polar coordinates  $(r, \theta)$  with origin at the centre of the aggregate, we suppose that the oxygen profile on the boundary is given by  $\phi(1, \theta) = \Phi_0 + \Phi(\theta)$ , where  $\Phi_0$  is a constant and  $\Phi$  has zero mean. Assuming that the aggregate is aerobic throughout, the oxygen profile inside the aggregate is given by

$$\psi(r, \theta) = \frac{1}{4} \alpha (r^2 - 1) + \Phi_0 + \sum_{n=1}^{\infty} r^n \left( \Phi_n^{(c)} \cos(n\theta) + \Phi_n^{(s)} \sin(n\theta) \right), \tag{7}$$

where the  $\Phi_n^{(c,s)}$  are the Fourier coefficients of the boundary data on  $A$ . Evidently (7) is monotonic increasing in  $r$ . An anaerobic core will therefore develop at the aggregate centre if

$$\alpha > 4(\Phi_0 - \tau), \tag{8}$$

a condition which depends on the mean oxygen profile around the aggregate boundary and the threshold parameter  $\tau$ . Moreover, (8) underscores the physical importance of the parameter  $\alpha$  as it essentially controls whether or not denitrification occurs within the soil. It will be helpful to place this into a physical context. Numerical values for the physical parameters in the model which are relevant to real soils have been estimated by various authors. In Table 1, we present typical values for rate of oxygen consumption,  $\lambda$ , the aggregate diffusivity  $D_2$ , and the threshold concentration for denitrification  $T$  extracted from a number of sources in the literature. The latter value is typically very small, and using the value due to Greenwood quoted in Table 1 we find  $\tau = 1.7 \times 10^{-5}$ . Consequently, we may reasonably assume that  $\tau \ll 1$ . Based on a typical atmospheric oxygen concentration of 21%, we will assume the value  $\phi_S = 0.21$  for the surface-level oxygen concentration. We will also take the value for the diffusivity of oxygen in air, namely  $D_1 = 0.2 \text{ cm}^2 \text{ s}^{-1}$ , as the reference value in region 1.

Since the diffusivity of oxygen in air is around ten thousand times the diffusivity of oxygen in water, selecting an appropriate value for  $\delta$  depends crucially on the water content in the region around the aggregates, and we expect a sharp contrast in the diffusivity ratio for dry and for water-logged soils. For example, using Currie [8]’s estimates for  $D_2$  in the case of a water-saturated aggregate and a dry aggregate from Table 1, we obtain  $\delta = 0.5 \times 10^{-5}$  and  $\delta = 0.05$ , respectively. Using instead Greenwood [11]’s estimate for  $D_2$  quoted in Table 1 for a saturated aggregate, we obtain  $\delta = 4.1 \times 10^{-5}$ .

**Table 1** Typical physical parameter values

Parameter	Source 1	Source 2	Source 3	Source 4
$a$	0.16 cm	–	5.01 cm	–
$\lambda$	$0.5 \times 10^{-5} \text{ s}^{-1}$	–	$2 \times 10^{-7} \text{ s}^{-1}$	–
$D_2$ (A)	$0.82 \times 10^{-5} \text{ cm}^2 \text{ s}^{-1}$	$1.05 \times 10^{-5} \text{ cm}^2 \text{ s}^{-1}$	–	$10^{-6} \text{ cm}^2 \text{ s}^{-1}$
$D_2$ (B)	–	–	–	$10^{-2} \text{ cm}^2 \text{ s}^{-1}$
$T$	$3 \times 10^{-6} \text{ mol L}^{-1}$	–	–	–

Source 1 refers to Greenwood [11, 12], Source 2 is Radford and Greenwood [27], Source 3 is Smith [28] and Source 4 is Currie [8]. The quoted values of the internal aggregate diffusivity  $D_2$  are for (A) a water-saturated aggregate and (B) a dry aggregate

Gardner [10], Allmaras et al. [1] and Smith [28] note that experiments based on aggregate sizes in British soils and in US soils have shown that aggregate size follows a log-normal distribution. Using the data quoted for curve (a) of figure 2 of Smith [28], we obtain an estimate for the mean aggregate size of 5.01 cm. This is the value quoted in Table 1. The smaller value of 0.16 cm obtained by Greenwood [11], and also quoted in Table 1, indicates the range of possible aggregate sizes, which may be found in different soils. Using the mean value provided by Smith for our aggregate size  $a$ , and taking the oxygen consumption rate  $\lambda = 2 \times 10^{-7} \text{ s}^{-1}$  extracted from Smith [28] in Table 1 together with the value  $D_2 = 10^{-6} \text{ cm}^2\text{s}^{-1}$  for a water-saturated aggregate from Currie [8], we obtain the estimate  $\alpha = 23.9$ . Using the smaller value of  $a = 0.16$  provided by Greenwood [11], we obtain  $\alpha = 0.02$ . It is clear, then, that quite a range of values of our dimensionless parameter  $\alpha$  is appropriate for a real soil.

It follows from the preceding discussion that for an aggregated soil comprising individual soil particles surrounded by air, the diffusion ratio is very small, and this suggests that mathematical progress can be made by seeking an asymptotic solution on this basis. This is examined in Sect. 3. For a non-aggregated soil, which is a homogeneous soil that contains one or more compact regions of decaying organic matter, such as dead leaves for example, the diffusion ratio  $\delta$  is expected to be of order unity. In this case, the solution to the problem (2)–(5), including the determination of the unknown boundary  $C$ , must be found numerically. This is discussed in Sect. 4.

### 3 Aggregated soil model: small diffusion ratio

As discussed in the previous section, in the case of an essentially dry soil containing water-saturated aggregates, the diffusion ratio  $\delta$  is expected to be very small. Working on this assumption, in this section we seek an asymptotic solution to (2)–(5), which is valid for small  $\delta$ . The remaining parameters in (6) are assumed to be  $O(1)$ .

Assuming  $\delta \ll 1$ , we expand the oxygen concentration in region 1 and region 2 by writing

$$\phi = \phi_0(x, y) + \delta \phi_1(x, y) + \dots, \quad \psi = \psi_0(x, y) + \delta \psi_1(x, y) + \dots \tag{9}$$

In region 1, the leading order concentration,  $\phi_0$ , satisfies Laplace’s equation with the conditions that  $\phi_0 = 1$  on  $y = 0$ , and  $\phi_{0y} \rightarrow 0$  as  $y \rightarrow -\infty$  and  $\mathbf{n} \cdot \nabla \phi_0 = 0$  on  $A$  so that the aggregate behaves as if it has an impermeable boundary. The solution is given by  $\phi_0 = 1$  everywhere in region 1. In region 2, the leading order problem is given by

$$\nabla^2 \psi_0 = \alpha, \tag{10}$$

with  $\psi_0 = 1$  on  $A$ . The other two boundary conditions require that  $\psi_0 = \tau$  and  $\mathbf{n} \cdot \nabla \psi_0 = 0$  on  $C$ , whose location is unknown. The symmetry of this problem suggests that to leading order  $C$  is a circle concentric with  $A$ , of radius  $c_0$  say. Using polar coordinates  $(r, \theta)$  with origin at the centre of the aggregate located at  $(x, y) = (0, -H)$ , we find

$$\psi_0 = \frac{1}{4}\alpha(r^2 - 1) + 1 - \frac{1}{2}\alpha c_0^2 \log r, \tag{11}$$

which satisfies the required Dirichlet condition at the outer boundary and the required Neumann condition at the inner boundary, namely  $\psi_{0r}(c_0) = 0$ . The remaining Dirichlet condition at the inner boundary requires the anaerobic core radius  $c_0$  to satisfy the equation

$$\tau - 1 - \frac{\alpha}{4}(c_0^2 - 1) + \frac{\alpha c_0^2}{2} \log c_0 = 0. \tag{12}$$

It is straightforward to show that this equation is satisfied by a real value of  $c_0$  lying in the physical range  $0 \leq c_0 \leq 1$ , provided that  $\alpha > 4(1 - \tau)$ . We note that this condition coincides with (8) on substituting  $\Phi_0 = 1$  as for the present case. Hence if  $\tau \ll 1$ , as stated above, then we essentially require that  $\alpha > 4$  for the presence of an anaerobic core; if  $0 \leq \alpha \leq 4$  the aggregate is aerobic throughout and no denitrification occurs. In Sect. 2, we obtained the physically realistic value  $\alpha = 23.9$ , and evidently an anaerobic core will exist in this case. Returning to dimensional variables the requirement  $\alpha > 4$  is equivalent to  $a > 2\sqrt{\phi_S D_2/\lambda}$ . Using the values  $\lambda = 2 \times 10^{-7} \text{ s}^{-1}$  and  $D_2 = 10^{-6} \text{ cm}^2\text{s}^{-1}$  quoted in Table 1, together with  $\phi_S = 0.21$ , we see that an aggregate will contain an anaerobic core if its radius exceeds 2.05 cm; otherwise, the rate of

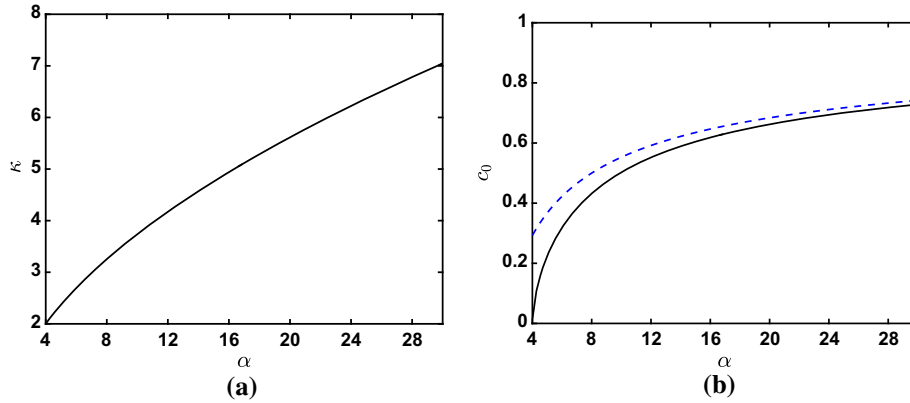


**Fig. 2** Results for  $\delta \ll 1$  when  $\tau = 0$ : **a**  $\kappa$  versus  $\alpha$ , and **b**  $c_0$  versus  $\alpha$ . The large  $\alpha$  asymptote  $c_0 = 1 - (2/\alpha)^{1/2}$  is shown with a broken line

oxygen uptake inside the aggregate is too weak for an anaerobic core to develop. The precise value of  $c_0$  may be determined by solving (12) numerically for a chosen set of parameter values. For large  $\alpha$ , it is easy to show that  $c_0 \sim 1 - \sqrt{(1 - \tau)} (2/\alpha)^{1/2} + \dots$  so that as  $\alpha$  increases the anaerobic core tends to fill the aggregate. We note in passing the similarity between the present leading order calculation and the textbook calculation for the development of a necrotic core inside a solid tumour with a known nutrient concentration on its boundary (e.g. [4]).

Assuming that  $\alpha > 4(1 - \tau)$ , we describe the *a priori* unknown location of the anaerobic core boundary  $C$  as  $r = c_0 + \delta c_1(\theta) + O(\delta^2)$ . For the first-order problem, it is convenient to introduce the new variable  $\hat{\phi}_1 = \phi_1/\kappa$ , where

$$\kappa = \alpha(1 - c_0^2)/2. \tag{13}$$

Taking into account the leading order solution discussed above, the problem for  $\hat{\phi}_1$  in region 1 is

$$\nabla^2 \hat{\phi}_1 = 0 \quad \text{with} \quad \begin{cases} \hat{\phi}_1 = 0 & \text{at } y = 0 \\ \hat{\phi}_{1y} \rightarrow 0 & \text{as } y \rightarrow -\infty \\ \hat{\phi}_{1r} = 1 & \text{at } r = 1. \end{cases} \tag{14}$$

Since  $\kappa > 0$  there is a net flux of oxygen into the aggregate at this order of approximation. Figure 2a, b shows how  $\kappa$  and  $c_0$  vary with  $\alpha$  when  $\tau = 0$  (recall that we expect  $\tau$  to be small in practice). It is interesting to note that for the physically reasonable value  $\alpha = 23.9$  quoted in Sect. 2, the leading order approximation to the anaerobic core radius,  $c_0$ , is well approximated by the large  $\alpha$  asymptotic formula. In this case,  $c_0 = 0.69$ , so that almost 70% of the aggregate is anaerobic.

The first-order problem in region 2 is

$$\nabla^2 \psi_1 = 0 \quad \text{with} \quad \begin{cases} \psi_1 = 0 & \text{at } r = c_0 \\ \psi_{1r} = -\alpha c_1 & \text{at } r = c_0; \end{cases} \tag{15}$$

and the two problems are coupled by the first of the two continuity conditions (3), which to first-order approximation requires that

$$\psi_1 = \phi_1(1, \theta). \tag{16}$$

In Sect. 3.1, we present an analytical solution of the problem for a single aggregate before turning our attention to the case of multiple aggregates in Sect. 3.2.

### 3.1 Single aggregate

Before proceeding to consider a network of aggregates making up an aggregated soil, it is of interest to examine the case of a single aggregate in isolation and to determine its effect on the ambient oxygen distribution. The first-order problem in region 1, namely (14), may be tackled by introducing an image aggregate above the ground surface and then employing bipolar coordinates (see Bocking [3] for details). An appealing alternative is to introduce an image aggregate as described and then to make use of the Villat formula from potential theory, which is applicable to problems with doubly-connected domains (e.g. [5,6]). Following the latter path, and writing  $z = x + iy$ , we seek a representation via a complex function,

$$w(z) = \hat{\phi}_1(x, y) + iv(x, y), \tag{17}$$

which is analytic in the region exterior to  $A$  and its image region  $A_I$ , obtained by reflecting  $A$  in the  $x$  axis. Furthermore, we demand that

$$v = \text{Im}(w) = \begin{cases} -s & \text{on } A, \\ s & \text{on } A_I, \end{cases} \tag{18}$$

where  $s$  denotes arc length around the boundary of either  $A$  or  $A_I$ , measured in the counterclockwise direction with  $s = 0$  at the lowermost point. Condition (18) has been derived by using the Cauchy–Riemann equations to recast the Neumann boundary condition on  $A$  in (14) and its counterpart on the image aggregate  $A_I$ . Using the terminology of fluid mechanics, according to (18) the aggregate is endowed with a nonzero circulation and this must be properly accounted for in the solution. Proceeding, we transform the physical domain in the  $z$ -plane to the annulus  $\rho < |\zeta| < 1$  in the  $\zeta$ -plane via the conformal mapping

$$\zeta = \rho^{1/2} \left( \frac{\mathcal{A} + iz}{\mathcal{A} - iz} \right), \quad \text{with } \mathcal{A}^2 = H^2 - 1, \quad \rho = \frac{H - \mathcal{A}}{H + \mathcal{A}}, \tag{19}$$

and define  $W(\zeta) \equiv w(z)$ . Under mapping (19), the circles  $A'$  at  $|\zeta| = 1$  and  $A'_I$  at  $|\zeta| = \rho$  are the  $\zeta$ -plane images of the circles  $A$  and  $A_I$ , respectively.

We seek a solution in the annular region  $\rho < |\zeta| < 1$  in the form

$$-iW(\zeta) = i \log(\zeta/\rho^{1/2}) - ig(\zeta), \tag{20}$$

where  $g(\zeta)$  is analytic in the annulus. Again using the terminology of fluid mechanics, we may interpret the first term in (20) as representing a point vortex of one sign located at  $z = -\mathcal{A}i$  (inside  $A$ ) and a point vortex of the opposite sign located at  $z = \mathcal{A}i$  (inside  $A_I$ ) in the  $z$ -plane. In this way, each of the aggregates is furnished with the necessary circulation alluded to above. To complete a solution which fulfils the boundary conditions (18), the analytic function  $g(\zeta)$  must be such that its real part satisfies

$$\text{Re}(-ig) = \begin{cases} (\tilde{\theta} - s) & \text{on } |\zeta| = 1, \\ (\tilde{\theta} - s) & \text{on } |\zeta| = \rho, \end{cases} \tag{21}$$

where  $\tilde{\theta}$  is the polar angle in the  $\zeta$  plane, with  $\tilde{\theta} = 0$  on the real  $\zeta$  axis. Notice that mapping (19) switches the direction of transit around  $A$  from counterclockwise in the  $z$ -plane to clockwise in the  $\zeta$ -plane and this accounts for the first terms on the right-hand sides of (21) being of the same sign on each of the two  $\zeta$ -image circles. The problem to find the analytic function  $g$  is of the modified Schwarz type: it demands a single-valued analytic function whose real part satisfies a prescribed condition on the domain boundary.

Using the Villat formula (e.g. Crowdy et al. [5], Crowdy [6]), the solution is given by

$$-ig(\zeta) = I_+(\zeta) - I_-(\zeta) + I_c + ig_0, \tag{22}$$

where  $g_0$  is a constant and

$$I_+(\zeta) = \frac{1}{2\pi i} \int_{|\zeta'|=1} K(\zeta/\zeta') (\tilde{\theta} - s) \frac{d\zeta'}{\zeta'}, \quad I_-(\zeta) = \frac{1}{2\pi i} \int_{|\zeta'|=\rho} K(\zeta/\zeta') (\tilde{\theta} - s) \frac{d\zeta'}{\zeta'}, \tag{23}$$

$$I_c = -\frac{1}{2\pi i} \int_{|\zeta'|=1} (\tilde{\theta} - s) \frac{d\zeta'}{\zeta'},$$

where

$$K(\zeta) = 1 - \frac{2\zeta}{Q(\zeta)} \frac{dQ}{d\zeta}, \quad Q(\zeta) = (1 - \zeta) \prod_{k=1}^{\infty} (1 - \rho^{2k}\zeta)(1 - \rho^{2k}\zeta^{-1}). \quad (24)$$

The arc distance around each circle needed in (23) may be computed using the formula

$$s = \int_{-\pi}^{\tilde{\theta}} |\zeta z'(\zeta)| d\tilde{\theta}. \quad (25)$$

When  $\zeta$  lies on either of the circles so that  $\zeta = \zeta'$  at some point in the range of integration in either  $I_+$  or  $I_-$ , the respective integral is to be interpreted in the Cauchy principal value sense. We also note that the compatibility condition for single valuedness, equation (6) in [5], is satisfied. The solution to the  $\hat{\phi}_1$  problem is obtained by taking the real part of  $w$  and choosing the constant  $g_0 = 0$  so that  $\hat{\phi}_1 = 0$  on  $y = 0$ . Independent confirmation of this solution has been obtained by checking first against the solution obtained using bipolar coordinates and second against a numerical solution obtained using the boundary-element method (see Bocking [3]).

Next we seek a solution to the first-order interior problem (15). Since the right-hand side of the continuity condition (16) is a periodic function, we may express it as a Fourier series and seek a solution to the unknown core boundary correction  $c_1(\theta)$  in the same form. Using the fact that the problem is symmetric about the vertical line  $x = 0$  passing through the aggregate centre, we may write the solution to the first-order exterior problem in the form

$$\phi_1(1, \theta) = \kappa\mu_0 + \kappa \sum_{n=1}^{\infty} \mu_n \sin(n\theta), \quad \mu_0 = \frac{1}{2\pi} \int_0^{2\pi} \hat{\phi}_1(1, \theta) d\theta, \quad (26)$$

where  $\mu_0$  is the mean value of  $\hat{\phi}_1$  on the boundary. We seek a solution to the interior problem (15) in the form

$$\psi_1 = A \log r + B + \sum_{n=1}^{\infty} (C_n r^n + D_n r^{-n}) \sin(n\theta), \quad c_1(\theta) = v_0 + \sum_{n=1}^{\infty} v_n \sin(n\theta), \quad (27)$$

where the constants  $A$ ,  $B$ ,  $C_n$ ,  $D_n$  and the coefficients  $v_n$  are to be determined. Of particular interest are the values  $v_n$ , which determine the first-order correction  $c_1$  to the anaerobic core radius. These are found to be

$$v_0 = \frac{\kappa\mu_0}{\alpha c_0 \log c_0}, \quad v_n = \frac{2n\kappa}{\alpha c_0 (c_0^n - c_0^{-n})} \mu_n \quad (n \neq 0). \quad (28)$$

To leading order the region exterior to the aggregate (region 1) is perfused with oxygen at the same concentration level as at the ground surface, so that  $\phi_0 = 1$ . Although the leading order oxygen distribution is uniform, the positioning of the aggregate inside region 1 is important. Intuitively, we expect the anaerobic core to be larger the deeper the aggregate is located underground. In the present analysis, the area  $\mathcal{A}$  of the anaerobic core inside the aggregate is given by

$$\mathcal{A} = \pi c_0^2 + \left( \frac{\pi \mu_0 (1 - c_0^2)}{\log c_0} \right) \delta + O(\delta^2). \quad (29)$$

The first term corresponds to the anaerobic core area for an aggregate in an infinite surround with a uniform oxygen concentration. By considering the following identity for the harmonic function  $\hat{\phi}_1$ , namely  $\nabla \cdot (\hat{\phi}_1 \nabla \hat{\phi}_1) = |\nabla \hat{\phi}_1|^2$ , and integrating over the domain of region 1 and applying the divergence theorem, we obtain

$$\mu_0 = -\frac{1}{2\pi} \int_A |\nabla \hat{\phi}_1|^2 dl < 0, \quad (30)$$

where  $l$  measures arc length around the boundary, and so the mean oxygen concentration around the aggregate perimeter  $A$  is negative. Therefore, since  $0 < c_0 < 1$ , the second term in (29) is positive and the area of the anaerobic core is increased from its value in an infinite surround.

Figure 3a shows the variation of  $\mu_0$  with depth  $H$ . The large-depth behaviour can be determined by recognising that when the aggregate is a long way below ground level, it can be represented by a point sink of



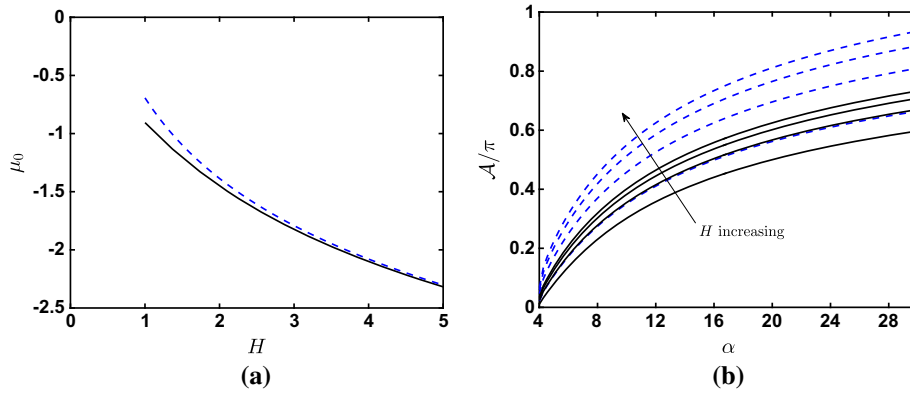


**Fig. 3** Results for  $\delta \ll 1$  when  $\tau = 0$ : **a** the dependence of  $\mu_0$  on dimensionless depth  $H$ . The result using the exact Villat formula is shown with a solid line, and the approximate result  $\mu_0 = -\log(2H)$  is shown with a dashed line. **b** The scaled anaerobic core area  $\mathcal{A}/\pi$  according to (29) for depths  $H = -1.00, -3.21, -5.42, -7.63$  ( $H$  increasing in the direction of the arrow as shown) for  $\delta = 0.05$  (solid lines) and  $\delta = 0.1$  (broken lines)

oxygen located at its centre  $\mathbf{x}_0 = (x_0, -H)$  such that  $\phi_1(\mathbf{x}) = \kappa \log(r/R)$ , where  $\mathbf{x} = (x, y)$ ,  $r = |\mathbf{x} - \mathbf{x}_0|$ ,  $R = |\mathbf{x} - \mathbf{x}'_0|$ , and  $\mathbf{x}'_0 = (x_0, H)$  is the location of an image source above ground level. The dashed line in Fig. 3a represents the value  $\mu_0 = -\log(2H)$ , which is calculated by substituting the point sink approximation for  $\hat{\phi}_1 = \phi_1/\kappa$  into the second equation in (26). The approximate result qualitatively reproduces the true behaviour over the whole range and quantitatively agrees closely with the correct value from a depth of only a few aggregate radii. The anaerobic core area scaled by the area of the aggregate,  $\mathcal{A}/\pi$ , is shown in Fig. 3b plotted against  $\alpha$ . The area is calculated using formula (29) neglecting the term  $O(\delta^2)$  and is shown for a sequence of dimensionless depths  $H$  and for two different small values of  $\delta$ . Evidently, the core area increases with depth, as anticipated.

### 3.2 Multiple aggregates

We now extend our discussion to describe an aggregated soil modelled as an organised network of  $M$  aggregates each with a circular boundary of unit dimensionless radius. The primary difficulty lies in determining the solution to the exterior problem in region 1. Here the first-order problem is given by (14) with the Neumann boundary condition represented by the last condition in (14) to be applied at each of the aggregate boundaries. We obtain the solution numerically using the boundary-element method. Following an established procedure for the Laplace equation (e.g. [26]), we first reformulate the problem for  $\phi_1$  as the integral equation of the second kind,

$$\frac{1}{2}\phi_1(\mathbf{x}_0) = -\kappa \int_A G^{(1)}(\mathbf{x}, \mathbf{x}_0) dl(\mathbf{x}) + \int_A \mathbf{n} \cdot \nabla G^{(1)}(\mathbf{x}, \mathbf{x}_0) \phi_1(\mathbf{x}) dl(\mathbf{x}), \tag{31}$$

where the point  $\mathbf{x}_0$  lies on  $A$ , which now represents the union of all of the individual aggregate boundaries. The Green's function is taken to be  $G^{(1)}(\mathbf{x}, \mathbf{x}_0) = (1/2\pi) \log(r/R)$ , where  $r = |\mathbf{x} - \mathbf{x}_0| = [(x - x_0)^2 + (y - y_0)^2]^{1/2}$  and  $R = [(x - x_0)^2 + (y + y_0)^2]^{1/2}$ ; note that  $G^{(1)}$  vanishes on  $y = 0$ .

The integral equation (31) is solved numerically by first discretizing each of the aggregate boundaries comprising  $A$  using a sequence of  $N$  straight-line boundary elements along which  $\phi_1$  is assumed to be constant. Enforcing (31) at the mid-point of each of these elements, and approximating the integrals using Gauss–Legendre quadrature, we obtain a set of  $NM$  algebraic equations for the  $NM$  unknown constant values of  $\phi_1$  on the elements. The linear system of equations is solved using Gaussian elimination. In implementing this procedure, we employed codes made freely available in the BEMLIB library [26]. In the results to be discussed below  $N$  was taken to be sufficiently large (typically between 100 and 200) to ensure that results are correct to the quoted number of decimal places. Once the exterior problem is solved, the analysis for the interior problem corresponding to (15) in each of the aggregates is similar to that presented above, and the same expression for area (29) applies with  $\mu_0$  representing the mean value of  $\phi_1/\kappa$  on the boundary of the aggregate in question, this value being available from the numerical solution of the exterior problem.

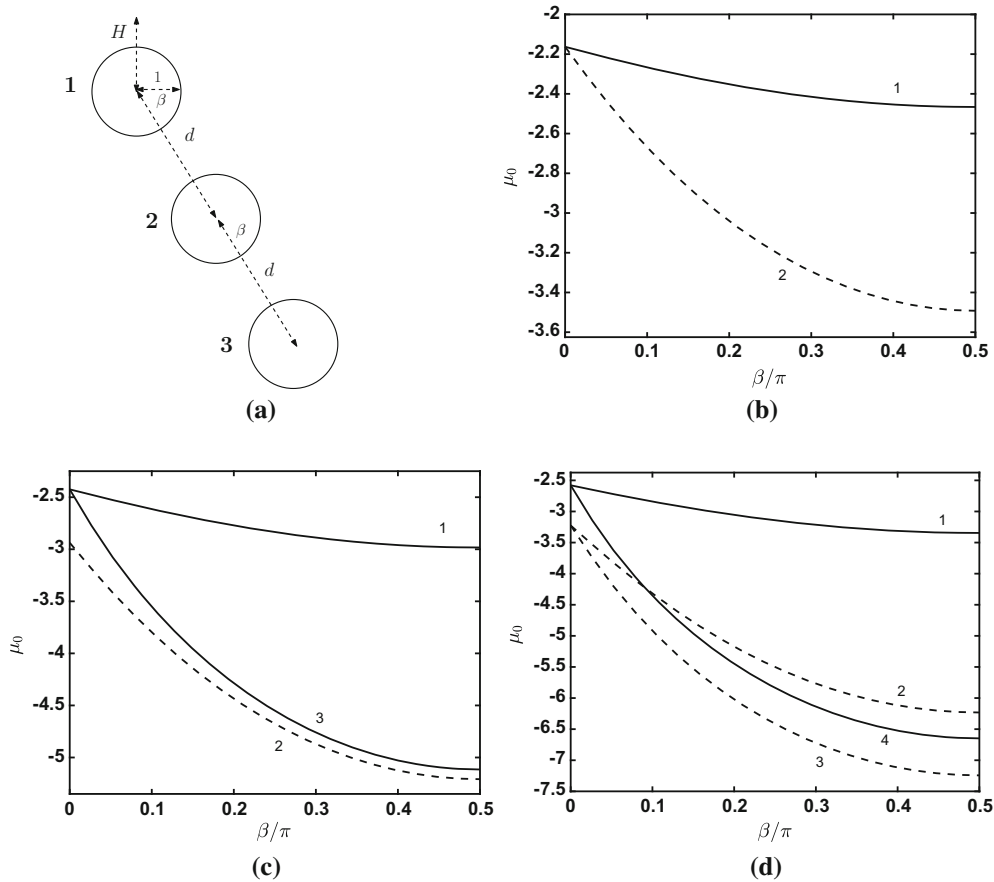


**Fig. 4** Multi-aggregate case for  $\delta \ll 1$ : **a** Illustrative sketch of three congruent aggregates separated by a dimensionless distance  $d$  at an angle  $\beta$ . The first aggregate has centre at dimensionless depth  $H$ . Panels (b–d) show the mean value  $\mu_0$  when **b** two aggregates are present, **c** three aggregates are present, and **d** four aggregates are present, each for varying orientation angle  $\beta/\pi$  with  $d = 3$  and  $H = 2$ . In each case, the curve labels refer to the aggregate number, which follows the convention illustrated in panel (a)

It is of interest to discuss how the number and relative arrangement of aggregates affect the mean value  $\mu_0$ . Consider a number of aggregates whose centres are located on a straight line inclined at an angle  $\beta$  to the horizontal and separated by a dimensionless distance  $d$ . The centre of the first aggregate, being the uppermost, is located at a dimensionless depth  $H$  below the ground level. Figure 4a illustrates the envisaged scenario in the case of three aggregates. Calculations were made for two aggregates, three aggregates and four aggregates. Figure 4b shows the mean value  $\mu_0$  for the two aggregate case,  $M = 2$ , over a range of orientation angles  $\beta$  and for fixed aggregate separation  $d = 3$ . Note for comparison that if the second aggregate is removed so that only the uppermost aggregate remains, then we find  $\mu_0 = -1.5$ . We observe in Fig. 4b that the value of  $|\mu_0|$  for both aggregates exceeds this value for a single aggregate. If  $d$  is increased, the value of  $\mu_0$  for aggregate 1 tends towards the value for a solitary aggregate,  $\mu_0 = -1.5$ , as might be expected. When  $\beta = 0$ , the same mean value  $\mu_0 = -2.2$  is computed for both aggregates. As the second aggregate moves beneath the first, it feels a sheltering effect which accords with intuition. In particular, as the inclination angle  $\beta$  reaches  $\pi/2$  the anaerobic core in aggregate 2 is significantly larger than that in aggregate 1.

Results for the same scenario but now with three aggregates ( $M = 3$ ) or four aggregates ( $M = 4$ ) are shown in panels (c) and (d) of the same figure. The mean value  $\mu_0$  decreases monotonically with  $\beta$  in all cases, and so the configuration for which the total anaerobic core area (summed over the aggregates) is maximised occurs when the aggregates are vertically aligned with  $\beta = \pi/2$ , as would be expected. For the three-aggregate case shown in Fig. 4c, two features are particularly striking. First, the differential in the value of  $\mu_0$  between aggregates 1 and 2, for example, is much greater in the vertical alignment than in the horizontal alignment. Second, in the vertical alignment the middle aggregate (2) has a larger anaerobic core than the bottom aggregate (3). For the case of four aggregates shown in Fig. 4d, we see that when in the horizontal alignment ( $\beta = 0$ ),

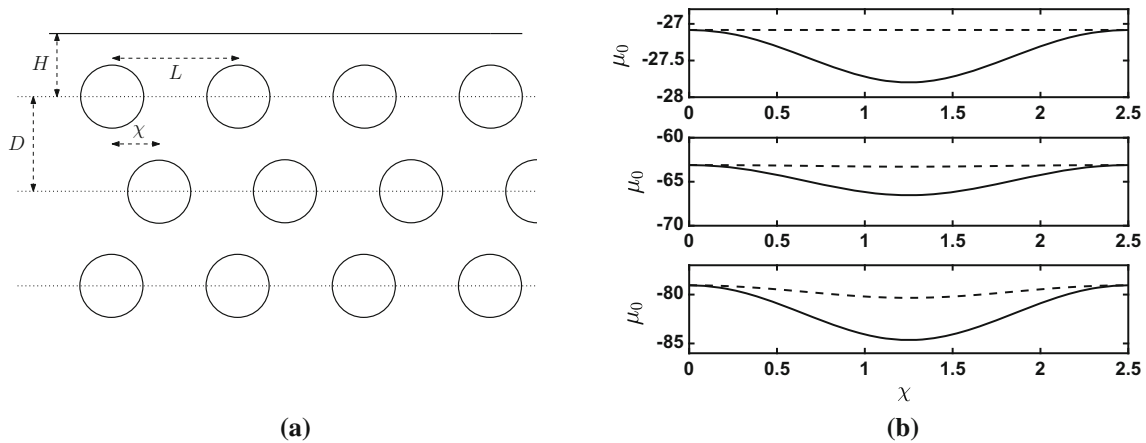


**Fig. 5** Multi-aggregate case for  $\delta \ll 1$ : **a** Sketch of a dislocated rectangular periodic lattice of aggregates located at a dimensionless distance  $H$  below ground with vertical row spacing  $D$ , and with one row shifted to the right by an amount  $0 \leq \chi \leq L$ . **b** The mean value  $\mu_0$  for the array in panel **(a)** with  $H = 1.5$ ,  $L = 2.5$  and  $D = (\sqrt{3}/2)L = 2.17$ . The middle or bottom row (solid or dashed line, respectively) is shifted horizontally by  $\chi$ . The value of  $\mu_0$  on one aggregate in the upper/middle/lower row is shown in the upper/middle/lower panel

the anaerobic core sizes for aggregates 1 and 4 are the same and those for aggregates 2 and 3 are the same, and moreover, the latter exceed the former. Evidently the innermost aggregates are sheltered by the outermost aggregates and receive less oxygen. Curiously, the anaerobic core size for aggregate 4 is larger than that for aggregate 2 when  $\beta \approx 0.3$ , but remains smaller than that for aggregate 3 even up to  $\beta = \pi/2$ . Consequently, for four aggregates in the vertically aligned position, the third aggregate down feels the greatest sheltering effect and receives the least oxygen.

An infinite network made up of a periodic repetition of an individual cluster of  $M$  aggregates provides a more realistic model of an aggregated soil. The periodic extension in the horizontal direction of the scenario just discussed is illustrated in Fig. 5a. The calculations for  $M$  aggregates in this periodically extended network are readily made by replacing  $G^{(1)}$  with the singly periodic Green's function,

$$G^{(3)} = \frac{1}{4\pi} \log \left\{ 2 \cosh [k(y + y_0)] - 2 \cos [k(x - x_0)] \right\} - \frac{1}{4\pi} \log \left\{ 2 \cosh [k(y - y_0)] - 2 \cos [k(x - x_0)] \right\}, \quad (32)$$

where  $k = 2\pi/L$  and  $L$  is the period. This function has been constructed so that  $G^{(3)} = 0$  on  $y = 0$ . It has the property  $\lim_{y \rightarrow -\infty} G^{(3)} = \text{constant}$ . Figure 5b shows calculated values of  $\mu_0$  for three rows of circular aggregates forming a rectangular lattice with periodicity  $L = 2.5$ . The first row is a dimensionless distance  $H = 1.5$  below ground level, and the rows are separated by a vertical distance  $D = (\sqrt{3}/2)L = 2.17$  dimensionless units. Either the middle or the bottom row suffers a dislocation in which one of the rows is shifted through a horizontal distance  $\chi$ , where  $0 < \chi < L$ . For  $\chi = 0$ , we have a regular rectangular lattice. Evidently the largest anaerobic cores are obtained when  $\chi = L/2$ , and the optimal state (under the stated conditions) in which the total anaerobic core area is maximised is obtained when the aggregates are equally spaced with their centres at the intersections of a uniform equilateral triangular network, corresponding to  $\chi = L/2$ . Investigating this equitriangular network further, we show in Fig. 6 how  $\mu_0$  depends on the network spacing  $L$ . Note that when  $L = 2.5$  the network corresponds to that shown in Fig. 5a for  $\chi = L/2$ . The results predict that the anaerobic core size in each aggregate will increase sharply as the network spacing is reduced and the aggregates become tightly packed. As the network spacing is increased, the mean value  $\mu_0$  for the first particle increases monotonically and eventually approaches the relevant value for an isolated aggregated at the appropriate depth (see Fig. 3a) as  $L \rightarrow \infty$ . This value is shown with a broken line in the figure. Interestingly, we see that for aggregates 2 and 3 the curves have a maximum so that there is an optimal spacing to minimise the size of the anaerobic cores in the second and the third rows of the network. Note that the maxima occur at similar, but not equal, values of  $L$ : for the case shown in the figure the maxima are at  $L = 35.8$  for row 2 and  $L = 37.6$  for row 3. We note that adding more rows to the network gives qualitatively similar results. For

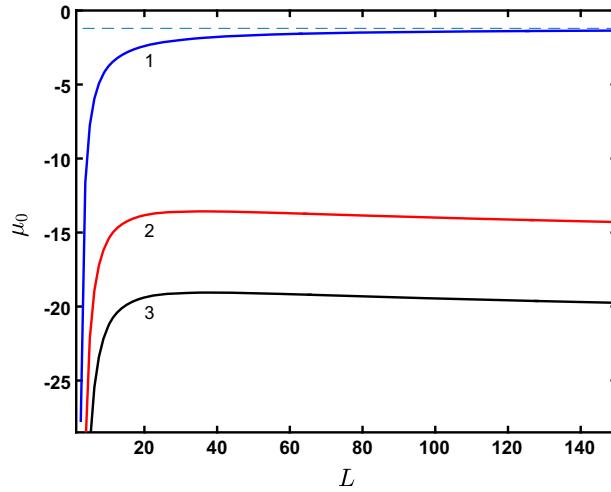


**Fig. 6** Multi-aggregate case for  $\delta \ll 1$ : The mean value  $\mu_0$  for a uniform triangular network with the aggregate centres equally spaced by an amount  $L$ , and the uppermost row placed at a depth  $H = 1.5$ . The curves 1, 2, 3 correspond to values of  $\mu_0$  on the aggregates labelled by the same numbers in Fig. 5a. The asymptote  $\mu_0 = -2.411$  for a solitary particle is shown with a broken line

example, including a fourth row we find results similar to those in Fig. 6 with an additional curve for aggregate 4 which is qualitatively similar to those for aggregates 2 and 3 and lying beneath both of them.

**4 Non-aggregated soil: arbitrary diffusion ratio**

For arbitrary values of the diffusion ratio  $\delta$ , we compute the solution to problem (2)–(5) numerically using the boundary-element method. First we reformulate the problem as a set of coupled integral equations. The formulation for the Laplace equation in region 1 is standard (e.g. Pozrikidis [26]). Introducing the new variable  $\hat{\phi} = \phi - 1$ , in region 1 and following the usual procedure, we obtain

$$\frac{1}{2}\hat{\phi}(\mathbf{x}_0) = - \int_A G^{(1)}(\mathbf{x}, \mathbf{x}_0) \mathbf{n} \cdot \nabla \hat{\phi}(\mathbf{x}) dl(\mathbf{x}) + \int_A \mathbf{n} \cdot \nabla G^{(1)}(\mathbf{x}, \mathbf{x}_0) \hat{\phi}(\mathbf{x}) dl(\mathbf{x}), \tag{33}$$

where  $\mathbf{x}_0$  lies on  $A$ , and  $\mathbf{n}$  is the unit normal to  $A$  pointing into region 1. The Green’s function  $G^{(1)}(\mathbf{x}, \mathbf{x}_0)$  was defined in the previous section.

To develop a similar integral formulation for the Poisson equation (4) in region 2, we start with Green’s second identity and integrate over region 2, denoted here by  $\Omega$ , to obtain

$$\begin{aligned} \psi(\mathbf{x}_0) = & - \int_{A,C} G^{(2)}(\mathbf{x}, \mathbf{x}_0) \mathbf{n} \cdot \nabla \psi(\mathbf{x}) dl(\mathbf{x}) + \int_{A,C} \psi(\mathbf{x}) \mathbf{n} \cdot \nabla G^{(2)}(\mathbf{x}, \mathbf{x}_0) dl(\mathbf{x}) \\ & - \alpha \iint_{\Omega} G^{(2)}(\mathbf{x}, \mathbf{x}_0) dx dy, \end{aligned} \tag{34}$$

where  $\mathbf{n}$  is the unit normal to  $A$  or  $C$  pointing into region 2 in either case, and  $G^{(2)}(\mathbf{x}, \mathbf{x}_0) = (1/2\pi) \log r$  is the free-space Green’s function with  $r = |\mathbf{x} - \mathbf{x}_0|$ . To recast the area integral in (34) as an integral around the domain boundary, we make use of Green’s theorem in the plane for a domain  $\Omega$  with boundary  $\partial\Omega$ ,

$$\oint_{\partial\Omega} (L dx + M dy) = \iint_{\Omega} (M_x - L_y) dx dy, \tag{35}$$

and choose

$$L(x, y) = -\frac{1}{8\pi} (\hat{y} - 2\hat{y} \log r), \quad M(x, y) = \frac{1}{8\pi} (\hat{x} - 2\hat{x} \log r), \tag{36}$$

where  $\hat{x} = x - x_0$  and  $\hat{y} = y - y_0$ , in order that  $M_x - L_y = G^{(2)}$ . Accordingly, we obtain a pair of integral equations in region 2 involving only integrals over the domain boundary. Writing  $\mathbf{a} = (L, M)$ , we have

$$\begin{aligned} \frac{1}{2}(\hat{\phi}(\mathbf{x}_0) + 1) = & -\frac{1}{\delta} \int_A G^{(2)} \mathbf{n} \cdot \nabla \hat{\phi}(\mathbf{x}) dl(\mathbf{x}) + \int_A^{PV} (\hat{\phi}(\mathbf{x}) + 1) \mathbf{n} \cdot \nabla G^{(2)} dl(\mathbf{x}) - \alpha \int_A \mathbf{a} \cdot \mathbf{t} dl(\mathbf{x}) \\ & - \int_C G^{(2)} \mathbf{n} \cdot \nabla \psi(\mathbf{x}) dl(\mathbf{x}) + \tau \int_C \mathbf{n} \cdot \nabla G^{(2)} dl(\mathbf{x}) + \alpha \int_C \mathbf{a} \cdot \mathbf{t} dl(\mathbf{x}), \end{aligned} \quad (37)$$

valid when  $\mathbf{x}_0$  is on  $A$ , and

$$\begin{aligned} \frac{1}{2}\tau = & -\frac{1}{\delta} \int_A G^{(2)} \mathbf{n} \cdot \nabla \hat{\phi}(\mathbf{x}) dl(\mathbf{x}) + \int_A (\hat{\phi}(\mathbf{x}) + 1) \mathbf{n} \cdot \nabla G^{(2)} dl(\mathbf{x}) - \alpha \int_A \mathbf{a} \cdot \mathbf{t} dl(\mathbf{x}) \\ & - \int_C G^{(2)} \mathbf{n} \cdot \nabla \psi(\mathbf{x}) dl(\mathbf{x}) + \tau \int_C^{PV} \mathbf{n} \cdot \nabla G^{(2)} dl(\mathbf{x}) + \alpha \int_C \mathbf{a} \cdot \mathbf{t} dl(\mathbf{x}), \end{aligned} \quad (38)$$

valid when  $\mathbf{x}_0$  is on  $C$ . The superscript  $PV$  indicates that an integral should be interpreted in the Cauchy principal value sense. The unit tangent vector  $\mathbf{t}$  points in the direction of increasing arc length  $l$  along a given boundary. We have made use of the continuity conditions (3) in deriving (37) and (38).

Our goal is to solve (33) together with (37) and (38) to determine the boundary concentration levels of  $\hat{\phi}$  and  $\psi$  and to determine the shape and location of the unknown anaerobic core boundary  $C$ . To accomplish this, we first guess the location of  $C$  and discretise the individual integrals using straight-edged boundary elements, taking  $N$  elements each around  $A$  and  $C$ . Imposing each of the integral equations at the mid-points of the elements, we obtain  $3N$  linear algebraic equations for  $3N$  unknowns including  $\hat{\phi}$  and  $\mathbf{n} \cdot \nabla \hat{\phi}$  at the element mid-points on  $A$ , and  $\mathbf{n} \cdot \nabla \psi$  at the element mid-points on  $C$ . The equations are solved using Gaussian elimination. Once we have solved the linear system, we update the location of  $C$  to enforce the zero flux boundary condition. To do this, we perturb the location of each of the nodes at the joins of the boundary elements in turn by moving the node a small increment in the direction of the local outward normal vector. We then resolve the above system of integral equations for the perturbed core boundary and then iterate using Newton's method until  $\mathbf{n} \cdot \nabla \psi$  at each node is less than a prescribed tolerance.

Once we have solved the integral equations and determined the position and shape of  $C$ , we may find the oxygen concentration at any point in the interior of region 1 and region 2 using the expressions

$$\hat{\phi}(\mathbf{x}_0) = - \int_A G^{(1)} \mathbf{n} \cdot \nabla \hat{\phi}(\mathbf{x}) dl(\mathbf{x}) + \int_A \hat{\phi} \mathbf{n} \cdot \nabla G^{(1)} dl(\mathbf{x}), \quad (39)$$

for  $\mathbf{x}_0$  in the region 1, and

$$\begin{aligned} \psi(\mathbf{x}_0) = & - \int_A G^{(2)} \mathbf{n} \cdot \nabla \psi dl(\mathbf{x}) + \int_A \psi(\mathbf{x}) \mathbf{n} \cdot \nabla G^{(2)} dl(\mathbf{x}) - \alpha \int_A \mathbf{a} \cdot \mathbf{t} dl(\mathbf{x}) \\ & - \int_C G^{(2)} \mathbf{n} \cdot \nabla \psi(\mathbf{x}) dl(\mathbf{x}) + \tau \int_C \mathbf{n} \cdot \nabla G^{(2)} dl(\mathbf{x}) + \alpha \int_C \mathbf{a} \cdot \mathbf{t} dl(\mathbf{x}) \end{aligned} \quad (40)$$

for  $\mathbf{x}_0$  in region 2.

The preceding formulation is easily adapted to cater for multiple regions of oxygen-absorbing soil, and the case of more than one microbial hot spot will be considered below an aggregated soil. Physically relevant values of the dimensionless parameters are discussed in Sect. 2. Here we assume a small patch of microbial activity with the oxygen diffusivities taken to be broadly the same in both the interior and the exterior of the patch. Therefore, we consider a range of values for  $\delta$  but with a focus on the case  $\delta = 1$ . Since, as discussed in Sect. 3, the critical oxygen level for denitrification to occur is very small, so that  $\tau \ll 1$ , for computational purposes we simply set  $\tau = 0$  throughout the remainder of this section.

#### 4.1 Results

We present numerical results computed using the boundary-element method for arbitrary values of  $\delta$ . Accordingly, we assume that the whole of the underground domain  $y < 0$  is densely occupied with soil and that oxygen depletion occurs through high microbial activity in isolated regions which is much more significant

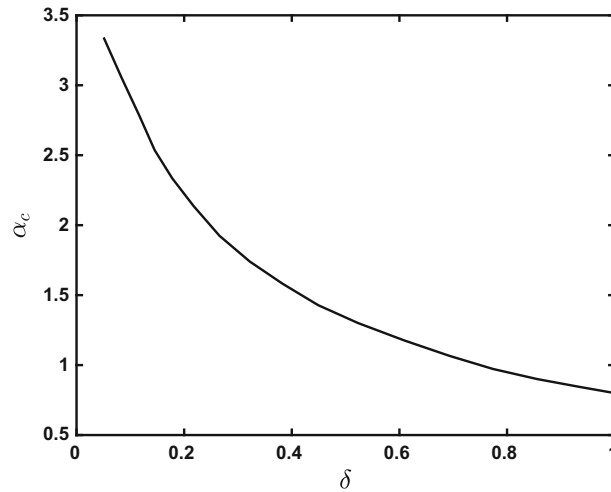


**Fig. 7** Dependence of the threshold value of  $\alpha$  for the appearance of an anaerobic core on the diffusion ratio,  $\delta$ , for the case  $\tau = 0$  and  $H = 4$ . An anaerobic core is present when  $\alpha > \alpha_c$

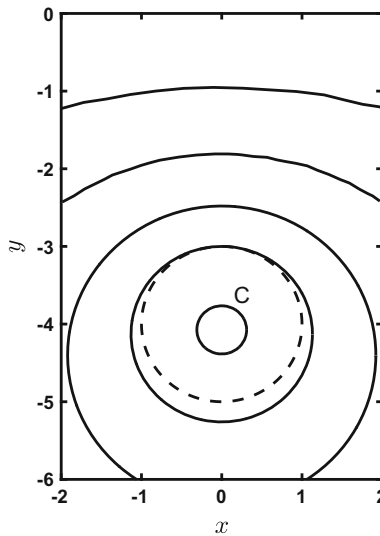


**Fig. 8** Contours of oxygen concentration for a non-aggregated soil with  $\alpha = 0.91$ ,  $\delta = 1$ , and  $\tau = 0$ . A circular area of high microbial activity, whose boundary is indicated by the broken line, at depth  $H = 4$  has depleted the surrounding oxygen levels. Contours are shown in steps of 0.2 between 0 and 1. The label  $C$  marks the boundary of the anaerobic core

than the activity in the surrounding area. Consistent with the formulation in Sect. 2, we refer to the surrounding soil as region 1 and a region populated by micro-organisms as region 2.

The asymptotic analysis presented in Sect. 3 for small values of the diffusion ratio  $\delta$  predicts that an anaerobic core will develop inside an aggregate when  $\alpha$  exceeds a critical value which depends on the oxygen concentration on the boundary (condition 8). We find that this critical value, which we label  $\alpha_c$ , decreases as  $\delta$  increases. This is illustrated by the sample calculation presented in Fig. 7. Assuming the presence of a small microbial patch of size  $a = 0.5\text{cm}$ , and using the physical parameter values cited in Sect. 2, we obtain  $\alpha = 0.91$ . Taking this value for  $\alpha = 0.91$  and setting  $\delta = 1$ , we deduce that if the patch is located at dimensionless depth  $H = 4$ , then an anaerobic core will be present. Contours of oxygen concentration for such a patch are shown in Fig. 8. The circular boundary of the microbial patch is shown in the figure with a broken line. The innermost contour, where the oxygen level is zero, corresponds to the anaerobic core boundary  $C$ . In contrast to the small  $\delta$  case studied in Sect. 3, where the oxygen distribution is essentially uniform in region 1, here the oxygen distribution around the patch is substantially altered from that at ground level. As would be expected, the anaerobic core grows in size if the microbial patch is moved to a greater depth. This

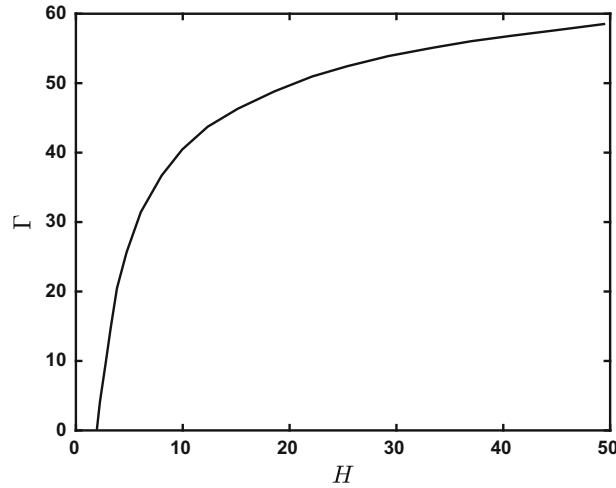


**Fig. 9** Variation of the anaerobic fraction  $\Gamma$  with depth  $H$  for the case  $\alpha = 0.91$ ,  $\delta = 1$  and  $\tau = 0$

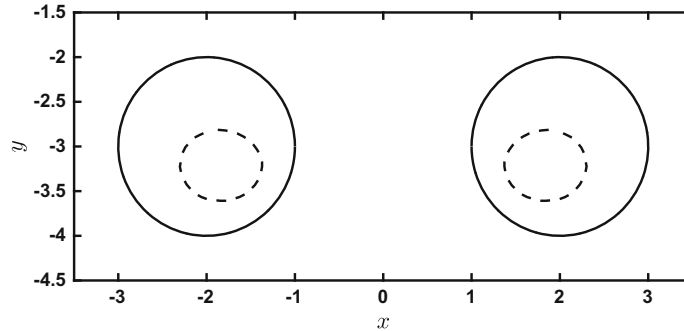


**Fig. 10** Anaerobic core boundaries  $C$ , shown with broken lines, for two horizontally aligned microbial patches, shown with solid lines, at depth  $H = 3$  for  $\alpha = 0.91$ ,  $\delta = 1$ , and  $\tau = 0$

is illustrated in Fig. 9, where the anaerobic fraction  $\Gamma$ , defined as the area of the anaerobic core divided by the area of the microbial patch, is plotted against depth  $H$ . It can be seen that the size of the anaerobic core grows progressively more slowly as the depth increases. When the patch is near to the ground surface, the anaerobic core is displaced a little way below the centre of the circular patch. As the depth  $H$  increases, the core boundary  $C$  tends to become circular and concentric with the boundary  $A$  as would be the case in a soil of infinite extent.

When multiple hotspot regions are present, we find that in general the anaerobic core within each region is larger than it would be if the region were in isolation at the same position and under otherwise identical conditions. A case with two microbial patches aligned horizontally is shown in Fig. 10. Here an anaerobic core is present within each region only because of the presence of the other patch. (For the conditions of this figure, a solitary patch at the same depth has no anaerobic core.) A vertical alignment of either two or three patches is shown in Fig. 11. For the two-patch case in Fig. 11a, it is clear that the size of the anaerobic core in the lower patch is considerably larger than that in the upper patch. This is in line with the sheltering effect felt discussed in Sect. 3 for an aggregated soil. The three-patch case in Fig. 11b has the smallest anaerobic core in the uppermost patch and a larger anaerobic core in the central patch than the lowermost patch. The latter is in line with the findings of the asymptotic theory of Sect. 3 (see Fig. 4c).

### 5 Discussion

We have presented a mathematical model of the oxygen depletion in soil aggregates. Our motivation has been to estimate the level of denitrification taking place in underground regions which have become depleted of oxygen by calculating the area of the anaerobic cores within aggregates. An anaerobic core develops inside

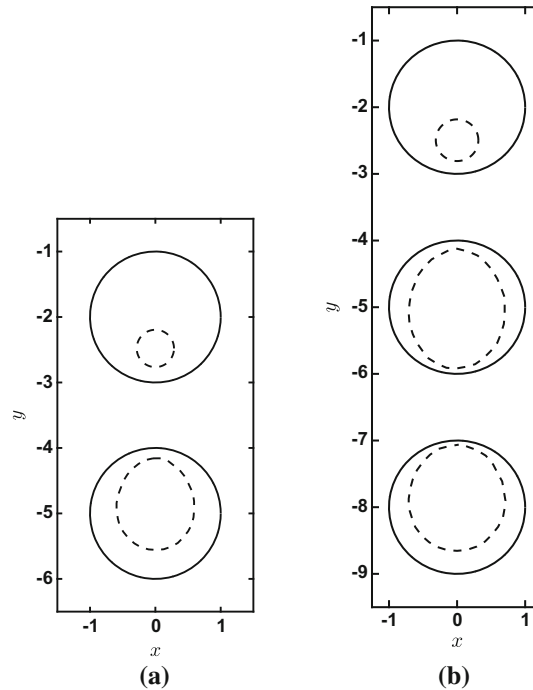


**Fig. 11**  $\alpha = 0.91$ ,  $\delta = 1$  and  $\tau = 0$ : **a** The anaerobic core boundaries  $C$ , shown with broken lines, for two vertically aligned microbial patches, shown with solid lines, with centres at  $y = -2$  and  $y = -5$ . **b** The anaerobic core boundaries, shown with broken lines, for three vertically aligned patches, shown with solid lines, with centres at  $y = -2$ ,  $-5$  and  $-8$ . The area fractions of the anaerobic cores are **a** 0.08 and 0.21 for the upper and lower patches, respectively, and **b** 0.1, 0.63 and 0.56 for the upper/middle/lower patches, respectively

an individual aggregate if the oxygen concentration on the surface of the aggregate is not large enough to allow microbes to maintain normal respiration. In particular, an anaerobic core appears when the interior concentration falls below a threshold level.

Isolated aggregates, multiple aggregates, and an infinite array of aggregates comprising a periodic network have been considered. Both aggregated and non-aggregated soils have been examined. In the case of an aggregated soil, the ground is viewed as comprising an array of individual particles or aggregates, inside which oxygen is depleted, that is surrounded by air (or water in the case of a saturated soil) in which oxygen diffuses but is not extracted. A non-aggregated soil views the ground as an essentially homogenous soil which contains localised hot spots of microbial activity. Our results have been presented with particular reference to the dimensionless depth at which an aggregate is located (taken as the ratio of the actual depth to the radius of the assumed circular aggregate), the oxygen diffusivity ratio  $\delta$  between the aggregate interior and its exterior, and the dimensionless parameter  $\alpha$ , which encapsulates the combined effects of aggregate size, rate of oxygen depletion, oxygen diffusivity inside the aggregate, and the ground-surface oxygen concentration. In particular, anaerobic sites appear within individual soil aggregates, or microbial patches, if  $\alpha$  exceeds a critical value. From a practical point of view, it seems reasonable to assume that one has some control over the aggregate size, by tilling the soil, for example, and hence some practical control over the value of  $\alpha$ .

For an aggregated soil, the oxygen diffusivity ratio between the air (or water) in the surround and the aggregate itself is small and mathematical progress was made on this basis. At leading order the oxygen concentration around the aggregates is constant and so each behaves as if embedded in an infinite medium with a constant oxygen concentration. Consequently, the anaerobic core inside each aggregate is circular to leading order. At first order, the location of an aggregate below the surface plays a role and acts to increase the core size with depth, as would be expected. For a solitary aggregate, we derived an explicit formula for the first-order correction to the anaerobic core size in terms of the mean concentration of oxygen on the aggregate boundary. The latter was calculated by solving the first-order problem outside the aggregate using the Villat formula from potential theory. We studied the case of two, three or four aggregates and demonstrated a sheltering effect whereby an individual aggregate's anaerobic core is increased in size if there are other aggregates lying



above it. Counter-intuitively, for a vertically arranged line of aggregates, it is not the lowermost that feels the greatest sheltering effect but the aggregate located one up from the bottom.

A model that includes a small collection of aggregates is naturally somewhat limited. In such a situation the oxygen concentration in the soil returns to the ground-surface level at a large enough distance away from the collection of aggregates. We constructed a more realistic representation of a soil by considering a periodic extension of an arrangement of a small number of aggregates to create an ordered network consisting of a finite number of rows each containing an infinite number of aggregates. With an infinite array like this, the oxygen concentration does not return to the ground-surface level at sufficient distance below the aggregates. As more rows are included in the network, so the anaerobic core size increases in the bottom row, and eventually we expect the anaerobic core to effectively occupy the entire aggregate so that the oxygen level some distance below the soil quickly drops well below the surface level. The drop in overall oxygen concentration with depth is more significant the lower the diffusivity in the region surrounding the aggregates. A smaller diffusivity ratio is expected if the surround is filled with water rather than air, as would be the case for a waterlogged soil. We would infer, then, that a waterlogged soil would have greater total anaerobic core area and hence produce a greater level of nitrous oxide through denitrification. This observation is in agreement with other reports in the literature, such as in [22], where it is noted that denitrification rates are significantly higher after rainfall.

By studying dislocations of a rectangular network of aggregates, we found that the anaerobic core within each aggregate reaches a maximum size when the aggregates are arranged at the nodes of an equitriangular network. Increasing the spacing between the nodes of the network has the effect of first decreasing the anaerobic core size in the lower rows of the network and then increasing it. This is in line with intuition, which suggests that the anaerobic core size will be large for a tightly packed network, but that it will decrease as the network spacing is increased, allowing greater aeration between aggregates. However, as the spacing is increased further, aggregates not on the top row move to greater and greater depth, and so the core size starts to increase. As a consequence, there is an optimal inter-node spacing, which may be selected to minimise the overall anaerobic core size in the network and hence minimise the level of denitrification taking place in the soil. This could indicate that a lower level of denitrification may occur in a well-ploughed field of soil than in a compacted soil.

For a non-aggregated soil, the ratio of oxygen diffusivity between a microbial patch, representing a hot spot of bacterial activity, and the surrounding soil is not small. In this case, we formulated the problem for the oxygen concentration in the interior of the microbial patch and in the surround as a set of integral equations, which we solved using the boundary-element method. The novelty of this formulation lies in its treatment of the Poisson equation to be solved inside an individual aggregate. Attention here was focused on the case of a small number of hotspot regions. For a single microbial region located at a fixed depth below ground, our computations showed that the value of  $\alpha$  at which an anaerobic core appears decreases monotonically with the oxygen diffusivity ratio  $\delta$ . As might be expected, when multiple hotspot regions are present, the anaerobic core size within each is larger than that which would have been found for the same region in isolation. This means in particular that denitrification may occur within a microbial region as a direct result of its proximity to another such region, where it would not have occurred otherwise. This underscores the importance of the spatial distribution of such regions in influencing the overall level of denitrification taking place within a soil.

It should be emphasised that calculating the volume of soil which is anaerobic is not in itself sufficient to quantify the release of nitrous oxide into the atmosphere. As was pointed out by Smith et al. [30], the amount of  $N_2O$  which is actually released into the atmosphere depends strongly on the structure of the soil and on its water content. They note that a molecule of nitrous oxide gas created during the denitrification process stated in Eq. (1) is more likely to be released to the atmosphere, rather than converted to  $N_2$  in the final step of the process, if it can diffuse away from the production site and into an oxygenated pore; furthermore, denitrification that occurs at significant depth in a saturated soil is much more likely to complete the denitrification process and hence produce  $N_2$  rather than  $N_2O$ .

Finally, we remark that in this study we have concentrated on the effect of diffusion in describing the transport of oxygen within a model soil. As was noted in the Introduction, diffusion is expected to be the dominant mechanism for gaseous exchange. Nevertheless, it is not clear that the role of advection can be ignored in, say, a soil which has become saturated with water after a heavy rainfall event, and it would be interesting to extend the present model to account for this. This is left as a topic for future investigation.

**Acknowledgements** The authors would like to thank Professor D. Crowdy for an informative discussion on the use of the Villat formula. We are grateful to Prof. C. Pozrikidis for the BEMLIB [26] boundary-element codes which were used in part for this work. The work of MGB was supported by the EPSRC under Grant EP/K041134/1.

**Open Access** This article is distributed under the terms of the Creative Commons Attribution 4.0 International License (<http://creativecommons.org/licenses/by/4.0/>), which permits unrestricted use, distribution, and reproduction in any medium, provided you give appropriate credit to the original author(s) and the source, provide a link to the Creative Commons license, and indicate if changes were made.

## References

- Allmaras, R.R., Burwell, R.E., Voorhees, W.B., Larson, W.E.: Aggregate size distribution in the row zone of tillage experiments. *Soil Sci. Soc. Am. J.* **29**, 645–650 (1965)
- Arah, J.R.M., Smith, K.A.: Steady state denitrification in aggregated soils: a mathematical model. *J. Soil Sci.* **40**, 139–149 (1989)
- Bocking, C.: Modelling denitrification. In: Soil, PhD Thesis, University of East Anglia (2012)
- Britton, N.F.: *Essential Mathematical Biology*. Springer, New York (2002)
- Crowdy, D., Surana, A., Yick, K.-Y.: The irrotational motion generated by two planar stirrers in inviscid fluid. *Phys. Fluids* **19**, 018103 (2007)
- Crowdy, D.: The Schwarz problem in multiply connected domains and the Schottky–Klein prime function. *Complex Var. Ellip. Equ.* **53**, 221–236 (2008)
- Currie, J.A.: Gaseous diffusion in the aeration of aggregated soils. *Soil Sci.* **92**, 40–45 (1961)
- Currie, J.A.: Diffusion within soil microstructure a structural parameter for soils. *Euro. J. Soil Sci.* **16**, 279–289 (1965)
- Diaz-Zorita, M., Perfect, E., Grove, J.H.: Disruptive methods for assessing soil structure. *Soil Tillage Res.* **64**, 3–22 (2002)
- Gardner, W.R.: Representation of soil aggregate-size distribution by a logarithmic-normal distribution. *Soil Sci. Soc. Am. J.* **20**, 151–153 (1956)
- Greenwood, D.J.: The effect of oxygen concentration on the decomposition of organic materials in soil. *Plant Soil* **14**, 360–376 (1961)
- Greenwood, D.J.: Nitrification and nitrate dissimilation in soil. *Plant Soil* **18**, 378–391 (1962)
- Greenwood, D.J., Berry, G.: Aerobic respiration in soil crumbs. *Nature* **195**, 161–163 (1962)
- Groffman, P.M., Altabet, M.A., Böhlke, J.K., Butterbach-Bahl, K., David, M.B., Firestone, M.K., Giblin, A.E., Kana, T.M., Nielsen, L.P., Voytek, M.A.: Methods for measuring denitrification: diverse approaches to a difficult problem. *Ecol. Appl.* **16**, 2091–2122 (2006)
- Hillel, D.: *Introduction to Soil Physics*. Academic Press, New York (1982)
- Houghton, J.T., Ding, Y.D.J.G., Griggs, D.J., Nogue, M., van der Linden, P.J., Dai, X., Maskell, K., Johnson, C.A.: *Climate Change 2001: The Scientific Basis*. The Press Syndicate of the University of Cambridge, Cambridge (2001)
- Kanwar, R.S.: Analytical solutions of the transient state oxygen diffusion equation in soils with a production term. *J. Agron. Crop. Sci.* **156**, 101–109 (1986)
- Keen, B.A.: *The Physical Properties of the Soil*. Longman, London (1931)
- Knowles, R.: Denitrification. *Mircobiol. Rev.* **46**, 43–70 (1982)
- Kuzyakov, Y., Blagodatskaya, E.: Microbial hotspots and hot moments in soil: concept and review. *Soil Biol. Biochem.* **83**, 184–199 (2015)
- Leffelaar, P.A.: Simulation of partial anaerobiosis in a model soil in respect to denitrification. *Soil Sci.* **128**, 110–120 (1979)
- Li, C., Frolking, S., Frolking, T.A.: A model of nitrous oxide evolution from soil driven by rainfall events. I. Model structure and sensitivity. *J. Geophys. Res.* **97**, 9759–9776 (1992)
- Myrold, D.D., Tiedje, J.M.: Diffusional constraints on denitrification in soil. *Soil Sci. Soc. Am. J.* **49**, 651–657 (1985)
- Papendick, R.I., Runkles, J.R.: Transient-state oxygen diffusion in soil: I. The case when rate of oxygen consumption is constant. *Soil Sci.* **100**, 251–261 (1965)
- Perfect, E., Rasiyah, V., Kay, B.D.: Fractal dimension of soil aggregate-size distributions calculated by number and mass. *Soil Sci. Soc. Am. J.* **56**, 1407–1409 (1992)
- Pozrikidis, C.: *A Practical Guide to Boundary Element Methods with the Software Library BEMLIB*. Chapman and Hall/CRC, Boca Raton (2002)
- Radford, P.J., Greenwood, D.J.: The simulation of gaseous diffusion in soils. *J. Soil Sci.* **21**, 304–313 (1970)
- Smith, K.A.: A model of the extent of anaerobic zones in aggregated soils, and its potential application to estimates of denitrification. *J. Soil Sci.* **31**, 263–277 (1980)
- Smith, K.A.: The potential for feedback effects induced by global warming on emissions of nitrous oxide by soils. *Global Change Biol.* **3**, 327–338 (1997)
- Smith, K.A., Ball, T., Conen, F., Dobbie, K.E., Massheder, J., Rey, A.: Exchange of greenhouse gases between soil and atmosphere: interactions of soil physical factors and biological processes. *Eur. J. Soil Sci.* **54**, 779–791 (2003)